Metal–Organic Frameworks Hot Paper

Deutsche Ausgabe: DOI: 10.1002/ange.201602417
Internationale Ausgabe: DOI: 10.1002/anie.201602417

Controlled Generation of Singlet Oxygen in Living Cells with Tunable Ratios of the Photochromic Switch in Metal–Organic Frameworks

*Jihye Park, Qin Jiang, Dawei Feng, and Hong-Cai Zhou**

Abstract: *Development of a photosensitizing system that can reversibly control the generation of singlet oxygen ($^1O_2$) is of great interest for photodynamic therapy (PDT). Recently several photosensitizer–photochromic-switch dyads were reported as a potential means of the $^1O_2$ control in PDT. However, the delivery of such a homogeneous molecular dyad as designed (e.g., optimal molar ratio) is extremely challenging in living systems. Herein we show a Zr-MOF nanoplatform, demonstrating energy transfer-based $^1O_2$ controlled PDT. Our strategy allows for tuning the ratios between photosensitizer and the switch molecule, enabling maximum control of $^1O_2$ generation. Meanwhile, the MOF provides proximal placement of the functional entities for efficient intermolecular energy transfer. As a result, the MOF nanoparticle formulation showed enhanced PDT efficacy with superior $^1O_2$ control compared to that of homogeneous molecular analogues.*

The development of photosensitizers that can control the generation of singlet oxygen ($^1O_2$) has gained increasing attention in photodynamic therapy (PDT) research to reduce nonspecific damage from undesirably generated $^1O_2$.[1] PDT is a minimally invasive cancer treatment using cytotoxic $^1O_2$ that is generated by energy transfer (EnT) from an excited photosensitizer to molecular oxygen ($^3O_2$) upon appropriate light irradiation.[2] In this regard, the addition of an activation step provides another layer of selectivity on top of the localized nature of PDT, which is based on the directed light placement at the tumor site. As such, PDT with an activatable photosensitizer becomes an appealing therapeutic option whose sensitizing ability is activated in response to target stimuli.[1a,3] However, common activation mechanisms often involve irreversible or passive means. Therefore, the capability of controlling $^1O_2$ generation in a non-invasive and reversible manner is highly desired in photosensitizers.

To address this issue, a molecular dyad consisting of a porphyrinic photosensitizer and a dithienylethene (DTE) derivative as a molecular switch to reversibly turn on/off the $^1O_2$ generation was reported.[4] However, the delivery of such a complex system with multiple components is a formidable challenge in biological environments owing to the different molecular properties of each component, resulting in distinctive cell response or permeability.[5]

As a promising class of nanocarriers, metal–organic frameworks (MOFs) have captured extensive research interest because of their high porosity, synthetic tunability, and structural diversity.[6] Recently, MOFs have been studied as an efficient platform for energy transfer between linkers because of the highly accessible and spatially discrete linkers in the framework.[7] Herein we show energy-transfer-based $^1O_2$-controlled PDT using a Zr-MOF as a nanocarrier, in which the photosensitizing system installed in the MOF pores can control the $^1O_2$ generation using a photochromic switch. A widely employed photosensitizer, porphyrin[8] and a DTE derivative were successfully incorporated into the Zr-MOF with adjustable ratios. Our strategy, therefore, allows optimization of the energy transfer for $^1O_2$ control via fine-tuning of the ratios between two dyes incorporated into the MOF, as well as a successful delivery of the dyad into cells.

While incorporation of the desired functional molecules as linkers of the MOF could be straightforward, there are several major obstacles to be applied in living cells for the desired $^1O_2$ control. First, porphyrin and DTE derivatives are not suitable for constructing stable MOFs, compatible in physiological environments owing to their large sizes.[9] Moreover, classical mixed-linker strategies to incorporate multiple functionalities often employ labile coordination bonds, resulting in an instability of the framework in aqueous media.[10] In particular, the mixed-linker strategy usually yields a locked ratio between pre-designed functional molecules in the framework when the linkers are not topologically identical,[11] which could inherently limit the tuning of the system for targeted application. Therefore, a system, where the ratio between photosensitizer and photochromic switch can be tuned in the MOF, is highly desired to optimize the controllability of $^1O_2$ generation.

We chose UiO-66 as a base platform to build a photosensitizing MOF system that can realize a reversible control of $^1O_2$ generation for PDT. As an archetype of Zr-MOF, UiO-66 exhibits excellent chemical stability through coordination bonds between high valent Zr^{IV} and carboxylate.[12] Meanwhile, 2,12-connected **fcu-a** net of UiO-66 allows for many sub-networks, including **bcu-a**, **reo-a**, **hxg-a**, or high-defect frameworks.[13] Accompanied with the reduced connectivity, available coordination sites on Zr_6 clusters [$Zr_6O_4OH_4(COO)_{12}$] can be generated for the introduction of the functionalities via postsynthetic modification.[14] However,

[*] J. Park, Dr. D. Feng, Prof. Dr. H.-C. Zhou
Department of Chemistry
Texas A&M University
College Station, TX 77843 (USA)
E-mail: zhou@chem.tamu.edu
Homepage: http://www.chem.tamu.edu/rgroup/zhou/
Dr. Q. Jiang
Beijing National Laboratory for Molecular Sciences, Key Laboratory of Analytical Chemistry for Living Biosystems, Institute of Chemistry, the Chinese Academy of Sciences
Beijing, 100190 (P.R. China)
Supporting information and the ORCID identification number(s) for the author(s) of this article can be found under http://dx.doi.org/10.1002/anie.201602417.

the narrow pore window and small pore size of UiO-66 hinder the entrance of large DTE and porphyrin derivatives into the framework when postsynthetically approached. Therefore, we turned to an in situ insertion of these molecules into UiO-66 nanoparticles with a thermodynamic controlled synthesis.

To incorporate the photosensitizing system (dyad), derivatization of DTE and porphyrin cores to 1,2-bis(5-(4-carbonxyphenyl)-2-methylthien-3-yl)cyclopent-1-ene (BCDTE) and a free-base tetrakis(4-carboxyphenyl)-porphyrin (TCPP; Figure 1 a,b) was implemented for their potential coordination to Zr_6 cluster. Because the energy-transfer efficiency for switching on/off the $^1O_2$ generation is highly dependent on the molar ratios between the photosensitizer and photochromic switch,[4a] we designed photosensitizing systems in UiO-66 nanocarriers (**1**–**6**; Figure 2) by increasing the feed ratio of the BCDTE switch at a constant amount of TCPP for fine-tuning of the photosensitization and switching ability.

Interestingly, the optimized synthetic condition modified from the reported synthesis of UiO-66 nanoparticles,[15] where TCPP and BCDTE were simply added with other starting materials, could produce a pure phase of UiO-66 nanoparticles rather than a mixture of different MOFs. It is reasoned that the superior thermodynamic stability of UiO-66 inhibits possible formation of BCDTE-Zr-MOF, while the growth of TCPP-Zr-MOF, despite its high thermodynamic stability, was controlled by the low dose of TCPP.[16] Therefore, the single phase of UiO-66 can be targeted regardless of the complexity of the system. Meanwhile, both TCPP and BCDTE, containing multiple carboxylates, can readily participate in the coordination of Zr_6 clusters by partially substituting terephthalate linkers during the growth of UiO-66 (Figure 2 a). Once TCPP and BCDTE were installed inside the framework, the "ship-in-a-bottle" effect resulting from the small pore windows of UiO-66 and the robustness Zr-COO bonds can prevent the leaching of the inserted functionalities, thus maintaining the desired ratio after the synthesis.[17] More importantly, since TCPP and BCDTE are not serving as the linkers, our design allows for tuning the molar ratios between two dyes upon varying synthetic conditions, as well as the proximity of the dyes within the MOF nanoparticle for efficient energy transfer.

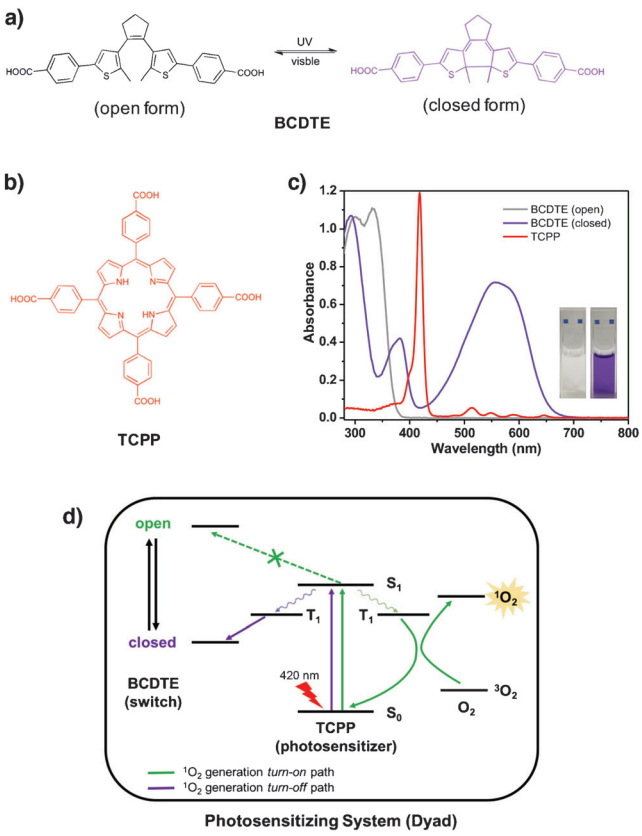

Figure 1. a) Chemical structures and photoisomerization of BCDTE. b) Chemical structure of TCPP. c) UV/Vis absorption spectra of BCDTE (30 μM) and TCPP (2 μM). Inset: photographs of solutions of BCDTE open (left) and closed (right) isomers. d) Proposed scheme of $^1O_2$ control via competitive energy-transfer pathways upon photoisomerization.

TEM and SEM images of **1**–**6** show approximately 70 nm of spherical nanoparticles with a high uniformity and a narrow size distribution (Figure 2 b and Figures S10–S12 in the Supporting Information). After confirming the phase purity of **1**–**6** (Figure 2 d), the ratio between BCDTE and TCPP in each sample was then determined by UV/Vis spectra (Table S6). Adjustable ratios of the incorporated molecules were further confirmed by XPS and EDS data (Supporting Information Sections 11 and 12). The homogeneity of the dyad in the samples was also confirmed by UV/Vis spectroscopy showing linear responses of each compound in the MOF (Figures S13 and S14) and TEM/EDS mapping results (Figure S5).

The $^1O_2$ generation controllability of the photosensitizing systems **1**–**6** was tested upon photoisomerization. A proposed mechanism for the control of $^1O_2$ generation is centered on competitive energy transfer pathways of TCPP emission between closed BCDTE and $^3O_2$ (Figure 1 d). Representative photoisomerization of BCDTE isomers was shown in Figure 1 c, exhibiting distinctive changes in absorption profile. Depending on the form of BCDTE isomers, therefore, the excited energy of TCPP can take different energy-transfer routes as shown in Figure 1 d. For instance, when the BCDTE switch is in the open form, the energy transfer occurs from ^{3}TCPP* to $^3O_2$, resulting in $^1O_2$ generation.[4a] On the other hand, the closed BCDTE upon UV irradiation quenches the $^1O_2$ generation due to possible EnT pathway to the closed BCDTE over $^3O_2$. To validate the feasibility of photoisomerization of BCDTE in UiO-66 nanoparticles, we prepared a sample only with BCDTE in UiO-66 (**7**) using the same synthetic strategy. Upon UV irradiation ($\lambda = 302$ nm) on the open form of BCDTE at UiO-66, the maximum absorbance of BCDTE was observed in 10–15 s, while prolonged UV irradiation led to a decrease in absorbance (Figure 3 a). The reverse reaction was also tested with a visible irradiation ($\lambda >$ 450 nm) and a near complete recovery was achieved in 15 min (Figure 3 b). It is worth noting that sample **7** shows much faster photoisomerization than that of other reported MOFs in which the photochromic molecules were incorporated as the linker.[7c,18] Knowing this, sample **6** was also tested for the photoisomerization. The reversible photoisomerization was

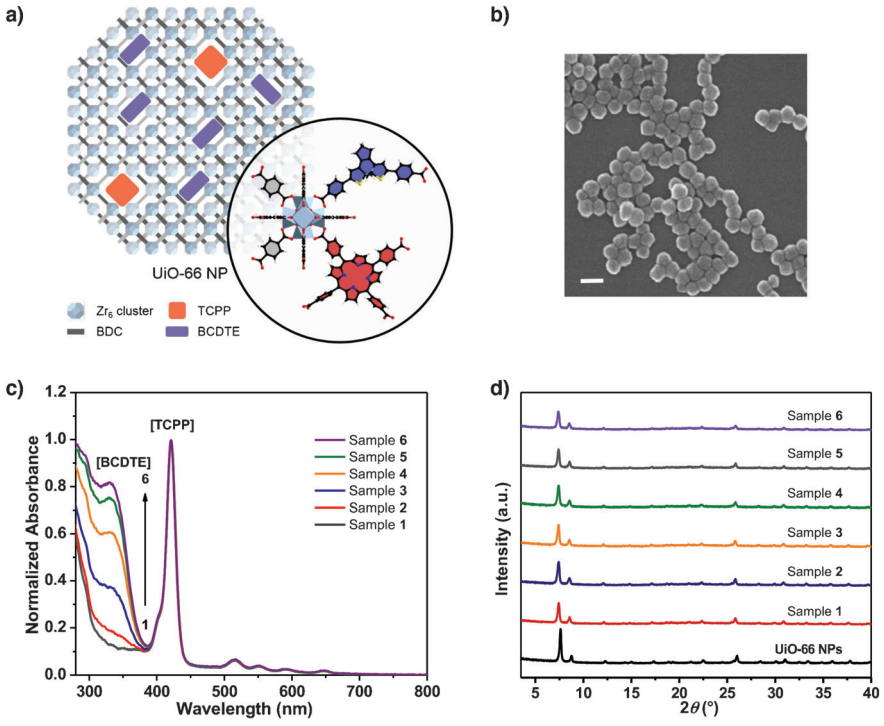

Figure 2. a) Defective structure of UiO-66 with inserted TCPP and BCDTE, and a proposed binding scheme of TCPP and BCDTE to a Zr_6 cluster. b) SEM image of sample **6**. Scale bar = 100 nm. c) UV/Vis absorption spectra of samples **1**–**6**, normalized at the same concentration of TCPP. d) PXRD patterns of UiO-66 nanoparticles and samples **1**–**6**.

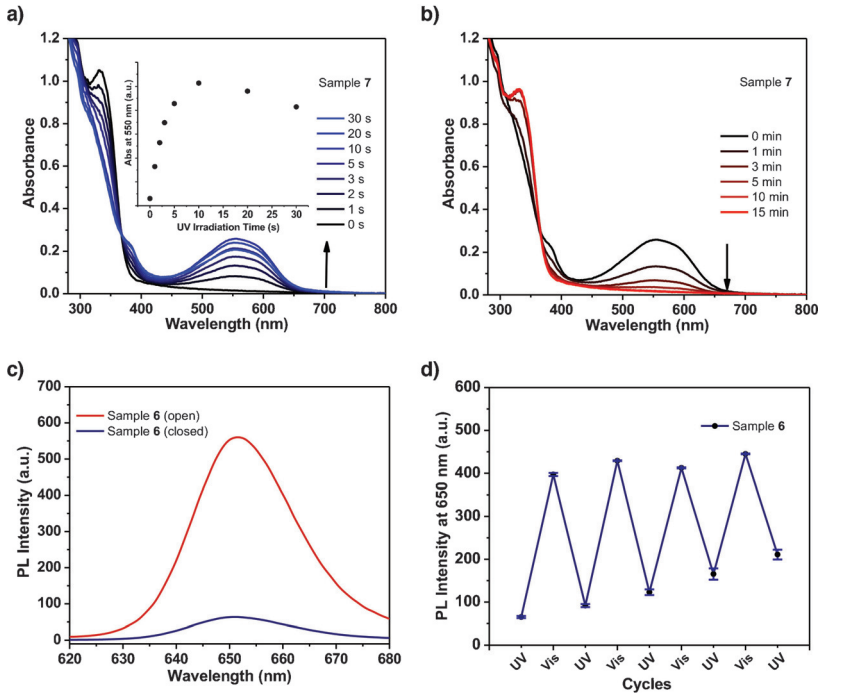

Figure 3. a) Changes in the UV/Vis absorption of sample **7** upon UV irradiation at 302 nm and b) recovery of UV/Vis absorption of **7** upon visible irradiation ($\lambda > 450$ nm with long pass filter) in DMF. c) Emission spectra of open and closed isomers of **6**. $\lambda_{ex} = 420$ nm. d) Changes in emission intensity of **6** at 650 nm over few cycles of photoisomerization. $\lambda_{ex} = 420$ nm.

clearly observed on a similar time frame while showing characteristic bands of both TCPP and BCDTE (Figure S4).

Because the emission of TCPP could strongly indicate the results of proposed energy transfer, the viability of regulating energy-transfer pathways in our system was then evaluated by fluorescence spectroscopy. The photosensitizing system **6** was chosen because the highest ratio of BCDTE over TCPP would result in the greatest quenching ability. The system was excited at the Soret band ($\lambda = 420$ nm) of TCPP to avoid possible intervention of the switching operation (Figure S28). The emission spectrum of **6** with the open switch (denoted as **6-o**) shows an emission maximum at 650 nm. To this sample, UV irradiation was applied to close the BCDTE switch in **6**. As expected, the emission at 650 nm was quenched upon UV irradiation, suggesting energy transfer occurred to the closed BCDTE as proposed (Figure 3c). Reverse photoisomerization of BCDTE was subsequently carried out with visible irradiation ($\lambda > 450$ nm), and a recovery of emission was achieved in 15 min, consistent with UV/Vis spectroscopic studies. Next, reversibility of the system was monitored by recording changes in emission intensity at 650 nm by alternating cycles of switching on/off. Slight loss of fatigue resistance was observed as cycles proceeded, which may be attributed to the substituent effect on DTE switch as studied in literature.[19] Nevertheless, in system **6**, the BCDTE to TCPP ratio can be as high as around 11:1, in which the emission of TCPP can be sufficiently quenched by a high concentration of the closed form of BCDTE.

After validating the reversible nature, [BCDTE]-dependent $^1O_2$ controllability was then examined with the closed form of BCDTE in each sample to compare the quenching efficiency of $^1O_2$ generation. The generated $^1O_2$ was monitored by turn-on fluorescence of singlet-oxygen sensor green (SOSG). Samples **1**–**6** (closed forms) were irradiated by 420 nm (100 mW cm^{-2}) to generate $^1O_2$. As expected, the $^1O_2$ quenching efficiency was proportional to the concentration of BCDTE switch

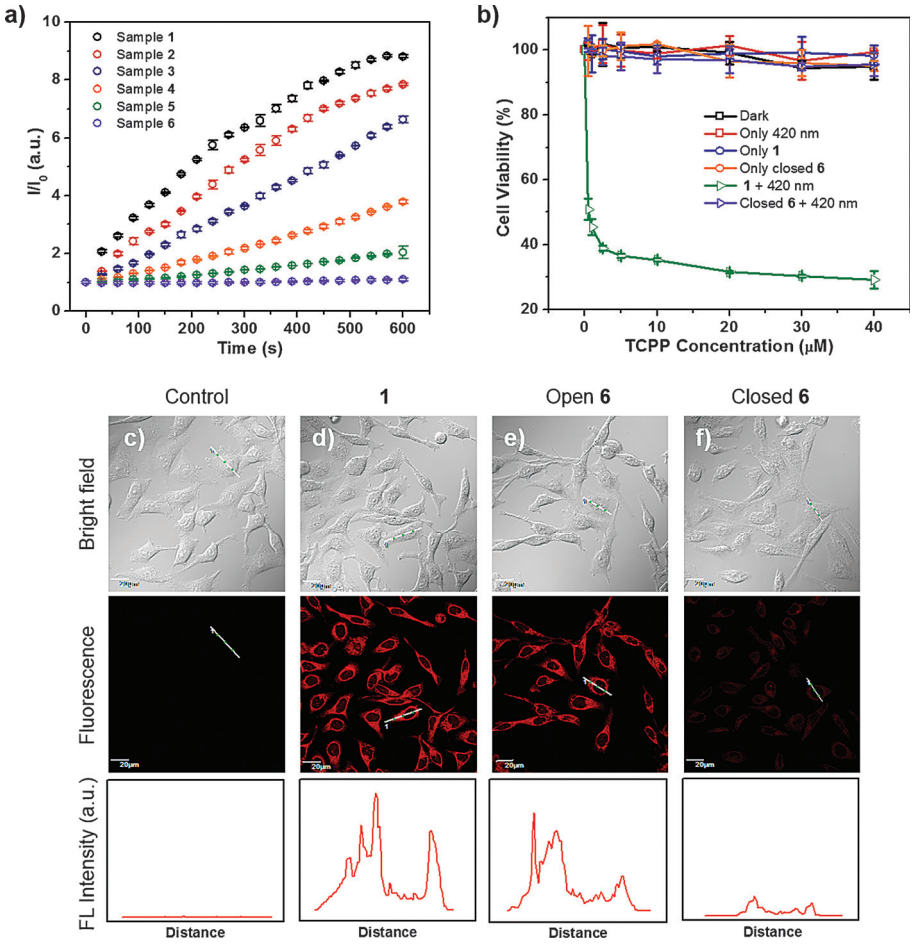

Figure 4. a) Irradiation time-dependent SOSG fluorescence response incubated with the closed form of samples **1**–**6** upon 420 nm irradiation for photosensitization. $\lambda_{ex} = 504$ nm, $\lambda_{em} = 550$ nm. b) In vitro PDT efficacy of sample **1** and **6-c** at various concentrations in B16 melanoma cells. Incubation time = 24 h. Irradiation time = 30 min. c–f) CLSM images of B16 cells treated with 20 μM of samples **1** and **6**, respectively (middle row). Cells treated with c) FBS free DMEM as a control; d) sample **1**; e) sample **6-o**; f) sample **6-c** for 60 min. The corresponding DIC images are shown at top row. Fluorescence intensity profiles within the line across B16 cells are shown at bottom row. Scale bars = 20 μm.

in each system (Figure 4a). In particular, **6** showed almost a near complete quenching of $^1O_2$ upon turn-off operation, suggesting energy transfer to $^3O_2$ was indeed more efficiently inhibited by the higher concentration of the closed BCDTE in **6**.

Having confirmed their $^1O_2$ controllability as well as effective photosensitization, we then evaluated the applicability of the systems in live cells. First, stability of the nanocarrier was examined in aqueous media where PXRD and dynamic light scattering (DLS) data showed no obvious destruction of the framework over a week (Figures S6 and S7). In vitro PDT studies were then carried out using B16 melanoma cells, a skin cancer model. Imaging capability of the material was examined by **1**, composed of only TCPP in UiO-66 nanoparticles, showing a strong red fluorescence, indicative of the emission from the photosensitizer (Figure 4d). Next, B16 cells were treated with **6-o** (the same TCPP equiv), exhibiting red emission as intense as **1**, which suggests the excited energy of TCPP was not disturbed by the open switch in **6** (Figure 4e). Switching ability of **6** was then validated by the cells incubated with the closed **6** (denoted as **6-c**), which shows a negligible fluorescence as a result of the proposed energy transfer to the closed form of BCDTE (Figure 4f). In addition, cell viability tests show low cytotoxicity of materials **1**–**6** to B16 cells at various concentrations for as long as 48 h (Figure S27).

Next, in vitro PDT efficacy was examined in B16 melanoma cells. While various control groups showed no apparent phototoxicity, sample **1** showed a significant PDT efficacy (Figure 4b). In particular, the cells treated with **6-c** showed almost no PDT efficacy, clearly supporting our hypothesis that energy-transfer-based control of $^1O_2$ generation was indeed realized in cell model (Figure 4b). To further confirm this concept, we directly compared PDT efficacy between **6-c** and **6-o**. As shown in Figure 5b, the PDT results indicate that switching operation can turn on $^1O_2$ generation in **6-o**, enabling desired control of $^1O_2$ for PDT through the photochromic switch. As a control experiment, the switching ability and ensuing PDT efficacy of a homogeneous mixture of BCDTE and TCPP molecules (without MOF nanoparticle formulation) were tested at the same concentrations as those in **6**. Interestingly, PDT efficacy of the small molecule system (open BCDTE/TCPP mixture) was less effective than that of **6-o**, further supporting the improved PDT efficacy by enhanced permeability and retention (EPR) effect, of which the improved delivery was achieved by the UiO-66 nanocarrier (Figure 5b,c). In particular, the results indicate that delivery of the mixture to target cells with their optimized molar ratio might be challenged presumably due to biological barriers (e.g., different cell permeability), suggested by noticeable loss of $^1O_2$ control (green in Figure 5c). Furthermore, the failure of maintaining effective local concentration of the homogeneous mixture of the dyad in the cells may also result in a significantly diminished control for $^1O_2$ quenching (Figure 5a). Therefore, in situ incorporation of multiple functionalities in MOF nanoparticle not only enhanced the delivery and PDT efficacy of the photosensitizing system over the molecular analogues, but also can be an attractive strategy to maintain the pre-designed system with multiple components (i.e., the optimized ratio) for desired applications.

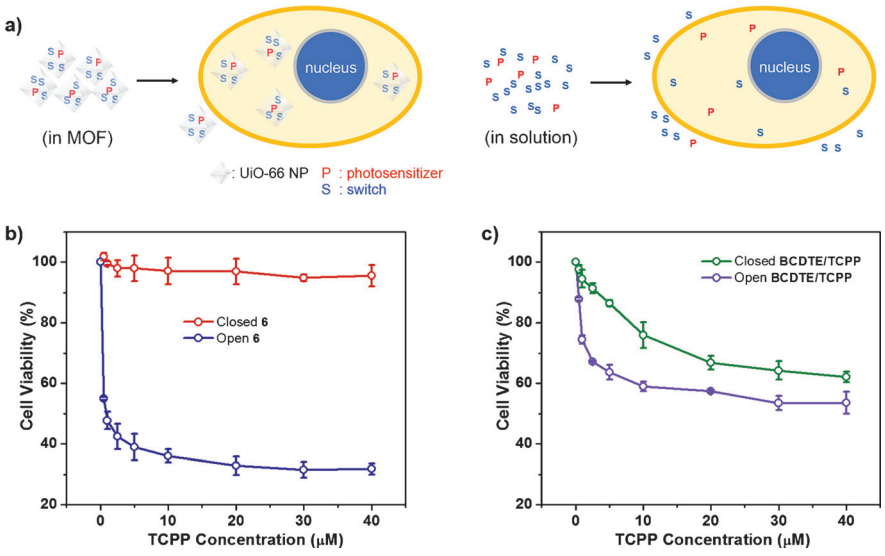

Figure 5. a) Proposed delivery of the photosensitizing system (BCDTE and TCPP) via MOF nanoparticle formulation (left) and a mixture of small molecules in solution (right). b) in vitro PDT efficacy between **6-c** and **6-o** at various concentrations in B16 cells upon irradiation at 420 nm. Incubation time = 24 h. Irradiation time = 30 min. c) in vitro PDT efficacy between open and closed forms of free BCDTE/TCPP mixture at various concentrations in B16 cells upon irradiation at 420 nm. Incubation time = 24 h. Irradiation time = 30 min.

In summary, our strategy of the in situ incorporation of the multiple functionalities in the MOF nanoparticle has been successfully demonstrated with a tunable ratio of the photochromic switch for the control of $^1O_2$ generation. This method also shows great potential for protected delivery of an integrated photosensitizing system as desired, allowing enhanced in vitro PDT efficacy with superior controllability of $^1O_2$ generation, using a MOF formulation compared to that of homogeneous mixture of the dyad.

Acknowledgements

The syntheses of MOFs and their characterizations were supported as part of the Center for Gas Separations Relevant to Clean Energy Technologies, an Energy Frontier Research Center funded by the U.S. Department of Energy, Office of Science, and Office of Basic Energy Sciences under Award Number DE-SC0001015. H.-C.Z. was supported by Texas A&M University. Also, use of the Texas A&M University Laboratory for Synthetic-Biologic Interactions, and the center for Physicochemical Analysis and Measurement at Institute of Chemistry, the Chinese Academy of Sciences, Beijing, are acknowledged. We gratefully acknowledge Dr. Zhangwen Wei for assistance in graphics and Ms. Shin Hye Ahn for helpful discussion.

Keywords: metal–organic frameworks · nanoparticles · photochromism · photodynamic therapy · singlet oxygen

How to cite: *Angew. Chem. Int. Ed.* **2016**, *55*, 7188–7193
Angew. Chem. **2016**, *128*, 7304–7309

[1] a) J. F. Lovell, T. W. B. Liu, J. Chen, G. Zheng, *Chem. Rev.* **2010**, *110*, 2839–2857; b) E. Cló, J. W. Snyder, P. R. Ogilby, K. V. Gothelf, *ChemBioChem* **2007**, *8*, 475–481.

[2] a) D. E. J. G. J. Dolmans, D. Fukumura, R. K. Jain, *Nat. Rev. Cancer* **2003**, *3*, 380–387; b) A. P. Castano, P. Mroz, M. R. Hamblin, *Nat. Rev. Cancer* **2006**, *6*, 535–545.

[3] a) S. S. Lucky, K. C. Soo, Y. Zhang, *Chem. Rev.* **2015**, *115*, 1990–2042; b) K. K. Ng, G. Zheng, *Chem. Rev.* **2015**, *115*, 11012–11042; c) P. Majumdar, R. Nomula, J. Z. Zhao, *J. Mater. Chem. C* **2014**, *2*, 5982–5997.

[4] a) L. Hou, X. Zhang, T. C. Pijper, W. R. Browne, B. L. Feringa, *J. Am. Chem. Soc.* **2014**, *136*, 910–913; b) *Molecular Switches*, Wiley-VCH, Weinheim, **2011**, Chap. 1; c) S. Kobatake, S. Takami, H. Muto, T. Ishikawa, M. Irie, *Nature* **2007**, *446*, 778–781; d) W. Szymański, J. M. Beierle, H. A. V. Kistemaker, W. A. Velema, B. L. Feringa, *Chem. Rev.* **2013**, *113*, 6114–6178; e) M. Irie, *Chem. Rev.* **2000**, *100*, 1685–1716.

[5] a) Y. N. Konan, R. Gurny, E. Allémann, *J. Photochem. Photobiol. B* **2002**, *66*, 89–106; b) A. Z. Wang, R. Langer, O. C. Farokhzad, *Annu. Rev. Med.* **2012**, *63*, 185–198.

[6] a) H.-C. Zhou, J. R. Long, O. M. Yaghi, *Chem. Rev.* **2012**, *112*, 673–674; b) P. Horcajada, R. Gref, T. Baati, P. K. Allan, G. Maurin, P. Couvreur, G. Ferey, R. E. Morris, C. Serre, *Chem. Rev.* **2012**, *112*, 1232–1268; c) C. He, D. Liu, W. Lin, *Chem. Rev.* **2015**, *115*, 11079–11108.

[7] a) C. Y. Lee, O. K. Farha, B. J. Hong, A. A. Sarjeant, S. T. Nguyen, J. T. Hupp, *J. Am. Chem. Soc.* **2011**, *133*, 15858–15861; b) K. Lu, C. He, W. Lin, *J. Am. Chem. Soc.* **2014**, *136*, 16712–16715; c) D. E. Williams, J. A. Rietman, J. M. Maier, R. Tan, A. B. Greytak, M. D. Smith, J. A. Krause, N. B. Shustova, *J. Am. Chem. Soc.* **2014**, *136*, 11886–11889; d) C. A. Kent, D. Liu, L. Ma, J. M. Papanikolas, T. J. Meyer, W. Lin, *J. Am. Chem. Soc.* **2011**, *133*, 12940–12943; e) H.-J. Son, S. Jin, S. Patwardhan, S. J. Wezenberg, N. C. Jeong, M. So, C. E. Wilmer, A. A. Sarjeant, G. C. Schatz, R. Q. Snurr, O. K. Farha, G. P. Wiederrecht, J. T. Hupp, *J. Am. Chem. Soc.* **2013**, *135*, 862–869; f) A. Fateeva, P. A. Chater, C. P. Ireland, A. A. Tahir, Y. Z. Khimyak, P. V. Wiper, J. R. Darwent, M. J. Rosseinsky, *Angew. Chem. Int. Ed.* **2012**, *51*, 7440–7444; *Angew. Chem.* **2012**, *124*, 7558–7562; g) E. A. Dolgopolova, D. E. Williams, A. B. Greytak, A. M. Rice, M. D. Smith, J. A. Krause, N. B. Shustova, *Angew. Chem. Int. Ed.* **2015**, *54*, 13639–13643; *Angew. Chem.* **2015**, *127*, 13843–13847.

[8] M. C. DeRosa, R. J. Crutchley, *Coord. Chem. Rev.* **2002**, *233–234*, 351–371.

[9] J. Park, D. Feng, S. Yuan, H. C. Zhou, *Angew. Chem. Int. Ed.* **2015**, *54*, 430–435; *Angew. Chem.* **2015**, *127*, 440–445.

[10] K. Tan, N. Nijem, P. Canepa, Q. Gong, J. Li, T. Thonhauser, Y. J. Chabal, *Chem. Mater.* **2012**, *24*, 3153–3167.

[11] a) B.-Q. Ma, K. L. Mulfort, J. T. Hupp, *Inorg. Chem.* **2005**, *44*, 4912–4914; b) H. Furukawa, N. Ko, Y. B. Go, N. Aratani, S. B. Choi, E. Choi, A. Ö. Yazaydin, R. Q. Snurr, M. O'Keeffe, J. Kim, O. M. Yaghi, *Science* **2010**, *329*, 424–428; c) L. Liu, S. G. Telfer, *J. Am. Chem. Soc.* **2015**, *137*, 3901–3909.

[12] a) J. H. Cavka, S. Jakobsen, U. Olsbye, N. Guillou, C. Lamberti, S. Bordiga, K. P. Lillerud, *J. Am. Chem. Soc.* **2008**, *130*, 13850 – 13851; b) W. Morris, W. E. Briley, E. Auyeung, M. D. Cabezas, C. A. Mirkin, *J. Am. Chem. Soc.* **2014**, *136*, 7261 – 7264.

[13] a) M. J. Cliffe, W. Wan, X. Zou, P. A. Chater, A. K. Kleppe, M. G. Tucker, H. Wilhelm, N. P. Funnell, F.-X. Coudert, A. L. Goodwin, *Nat. Commun.* **2014**, *5*, 4176; b) H. Wu, Y. S. Chua, V. Krungleviciute, M. Tyagi, P. Chen, T. Yildirim, W. Zhou, *J. Am. Chem. Soc.* **2013**, *135*, 10525 – 10532; c) C. A. Trickett, K. J. Gagnon, S. Lee, F. Gándara, H.-B. Bürgi, O. M. Yaghi, *Angew. Chem. Int. Ed.* **2015**, *54*, 11162 – 11167; *Angew. Chem.* **2015**, *127*, 11314 – 11319; d) J. M. Taylor, T. Komatsu, S. Dekura, K. Otsubo, M. Takata, H. Kitagawa, *J. Am. Chem. Soc.* **2015**, *137*, 11498 – 11506.

[14] J. B. DeCoste, T. J. Demasky, M. J. Katz, O. K. Farha, J. T. Hupp, *New J. Chem.* **2015**, *39*, 2396 – 2399.

[15] a) Z. Hu, D. Zhao, *Dalton Trans.* **2015**, *44*, 19018 – 19040; b) A. Schaate, P. Roy, A. Godt, J. Lippke, F. Waltz, M. Wiebcke, P. Behrens, *Chem. Eur. J.* **2011**, *17*, 6643 – 6651.

[16] D. Feng, Z.-Y. Gu, Y.-P. Chen, J. Park, Z. Wei, Y. Sun, M. Bosch, S. Yuan, H.-C. Zhou, *J. Am. Chem. Soc.* **2014**, *136*, 17714 – 17717.

[17] J. Juan-Alcañiz, J. Gascon, F. Kapteijn, *J. Mater. Chem.* **2012**, *22*, 10102 – 10118.

[18] a) F. Luo, C. B. Fan, M. B. Luo, X. L. Wu, Y. Zhu, S. Z. Pu, W.-Y. Xu, G.-C. Guo, *Angew. Chem. Int. Ed.* **2014**, *53*, 9298 – 9301; *Angew. Chem.* **2014**, *126*, 9452 – 9455; b) I. M. Walton, J. M. Cox, C. A. Benson, D. G. Patel, Y.-S. Chen, J. B. Benedict, *New J. Chem.* **2016**, *40*, 101 – 106.

[19] M. Herder, B. M. Schmidt, L. Grubert, M. Pätzel, J. Schwarz, S. Hecht, *J. Am. Chem. Soc.* **2015**, *137*, 2738 – 2747.

Received: March 9, 2016
Published online: April 29, 2016

